NEW ROTOR AIRFOIL DESIGN PROCEDURE FOR UNSTEADY FLOW CONTROL

W.Geissler*, H.Sobieczky**,M.Trenker***

Deutsches Zentrum für Luft- und Raumfahrt e.V., Institut für Strömungsmechanik,

Bunsenstr. 10, D-37073 Göttingen, Germany

Abstract:

It has been shown recently that active on-blade devices for helicopter rotor blades like trailing edge flaps have considerable potential compared to Higher Harmonic (HHC) and Individual Blade Control (IBC) technologies to reduce noise and vibration levels and improve performance of the rotor. With the development of new actuator devices it is now feasible to consider also the actuation of a sealed leading edge flap to favorably influence dynamic stall characteristics.
The "Nose-Drooping" concept has already been shown to be a very efficient tool to reduce drag and pitching moment peaks without reducing lift during the dynamic stall process. The corresponding Geometry Generation and unsteady CFD software has now been extended to take into account the combination of both incidence and Mach number variation simultaneously, i.e. simulating advancing and retreating sides of the rotor disc. In the present paper it is outlined that a drooping device is used on the retreating side of the loop which will be realized in the near future on a wind tunnel model. In addition the airfoil is modified to improve transonic characteristics on the advancing side by means of transonic design methodologies.

Introduction

Within the scope of the german project AROSYS (Adaptive Rotor Systems) between DLR, ECD and DaimlerChrysler AG it has been decided to develop a wind tunnel model for the DLR Transonic Wind Tunnel, Göttingen (TWG) incorporating a drooping device. About 10% of the airfoil leading edge will be oscillating about the axis of rotation as indicated in Fig.1. The maximum deflection angle of the flap will be $\Theta=10^{o}$. The Piezo-Electric Actuator used for this investigation has successfully been tested during the RACT (Rotor Active Control Technology) project [1], driving a trailing edge flap of a similar model in the TWG Wind Tunnel facility. The actuator-nose-droop-model combination has already been tested successfully in a laboratory test by DaimlerChrysler AG Research and Technology, [2].
The present numerical investigation takes into account the geometry of the airfoil/leading edge flap (nose-droop) combination. The necessary software tools have already demonstrated their efficiency and physical relevance for the active trailing edge flap with good correspondence between experimental and numerical data [3].
In the drooping case the investigation is further extended to combine both incidence and Mach number variations, i.e. simulating advancing and retreating parts of the rotation loop simultaneously. To simulate the Mach number variation the airfoil is assumed to move in its own plane in a sinusoidal mode which is 180^{o} phase shifted compared to the incidence variation (pitching mode).
The aim of the present investigation is not only to influence separation (dynamic stall) on the retreating side but also try to reduce the strength and local excursion of the shock wave on the advancing side of the loop. Corresponding numerical tools are available [4], to reduce or even completely avoid the shock wave on an airfoil.

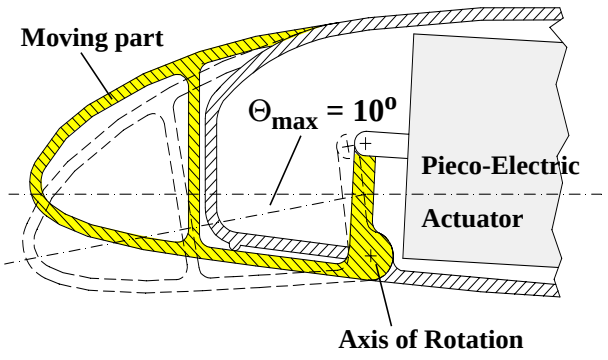

Fig. 1: Structural Realization of Nose-Droop Design

*Sr. Research Scientist

**Professor, Sr. Research Scientist

***Research Associate

2. Design Methodology.

The design of helicopter rotor airfoils is a matter of compromise:

- avoid or reduce separation up to high incidences
- avoid strong shock waves and shock induced separation up to high Mach numbers

to mention just the most important features a rotor airfoil should realize.

It is obvious that a rigid airfoil design can hardly represent these features sufficiently. Considerable improvements ar to be expected if the airfoil is changing its shape dynamically [5],[6].

It has been shown recently [7], that a completely flexible airfoil changing its camber line dynamically avoids dynamic stall completely and has in addition improved transonic flow characteristics. However the realization of such a design on a wind tunnel model or even on a full size rotor blade is not feasible nowadays.

In the present paper a design is therefore proposed which can be applied either on a wind tunnel model or on a full size blade applying **existing** technologies.

3. The Fictitious Gas Concept (FGC)

For the design of transonic airfoils the Fictitious Gas Concept [8] has shown considerable potential to develop either shock free or at least shock reduced airfoils at design conditions.

The FG-method uses a different set of equations for density and pressure inside the supersonic region i.e. assumes an artificial gas with always subsonic flow conditions. At the sonic line the fictitious gas region is smoothly connected to the outer subsonic perfect gas flow region.

These assumptions cause a major modification of the numerical code because the changes of pressure and density also change the equation of state correspondingly which leads to modified coefficient matrices involved in the implicit solution procedure, [9].

The FG-method has recently been applied for inviscid flows based on either potential or Euler equations, [8]. In the present study the unsteady Navier-Stokes equations have been solved [9] and the FG-concept has to be introduced into the viscous calculation procedure. This effort is not straightforward due to the fact, that pressure and density are no longer constant i.e. equal to the critical values along the sonic line as in the inviscid case. They are reduced inside the boundary layer. This reduction is not known analytically due to the fact that a turbulence model is involved. Therefore the values of p and ρ along the sonic line and the geometric shape of the fictitious gas region are determined numerically during the solution procedures of the Navier-Stokes code.

Fig. 2 shows schematically the result of this calculation. The FG-region is smooth and does not show any sign of a shock wave. But this solution is a fictitious one by defintion. Additional steps have to be carried out in order to get:

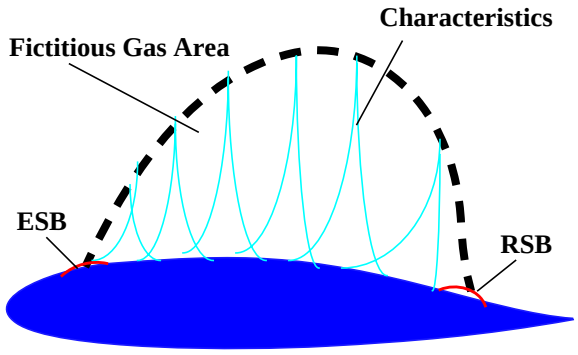

Fig.2: Fictitious Gas Concept (FGC)

a shock free airfoil design:

In a next step the FG-region (see Fig.2) is again filled with perfect gas and an inverse method of characteristics is applied with the boundary condition of M=1 along the outer border of the FG-region. The original airfoil surface will no longer be a stream surface and a modification has to be introduced to fulfill the boundary condition again.

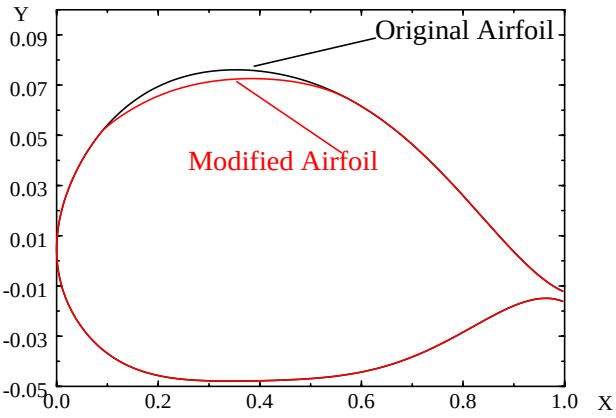

Fig. 3: Modified Airfoil Using FGC (Y-Enlarged)

Fig. 3 shows the result of the FG-design procedure. The modified airfoil shows a slight reduction of thickness along the supersonic area.

The amount of modification may be limited by introducing small surface bumps at both upstream (Expansion Shoulder Bump, ESB) and downstream (Recompression Shoulder Bump, RSB) ends of the supersonic region (see Fig. 2). Instead of flattening the upper surface of the airfoil and thus reducing the airfoil thickness which may be not an acceptable design, surface bumps have a similar effect: the curvature between the two bumps will be reduced, the shock wave will not be completely avoided but will be reduced in strength.

Some additional modifications have to be done to account

for the boundary layer displacement thickness. The FG-region (Fig.2) is assumed to touch the airfoil surface.
In a further step the FG-concept has also been introduced into the unsteady calculation procedure. This code feature makes it possible to calculate the unsteady flows with time-dependent variation of the fictitious gas region. Applying the method of characteristics for each time step would give information how the airfoil has to be modified **dynamically** to get a shock free design during the complete cycle. However in the present study it is realized that the airfoil is made almost shock free at the **maximum** Mach number keeping it rigid at other times. It will be shown that reduced shock strength will also be obtained at adjacent time instances.

4. Parameter Selection for Test Case

The numerical code, [9] has been extended to combine both pitching motion and translatory motion of the airfoil. The latter is simulating the Mach number variation. A characteristic set of parameters has been defined for the present numerical calculations:

a) Pitching motion about the quarter chord axis

$\alpha=10^o+10^o \sin(\omega^*T)$

b)Translatory motion (Mach number variation)

$M=0.50-0.23 \sin(\omega^*T)$

c) Parameters:

$\omega^*=0.3$ (referred to chord)

$Re=2*10^6$

The maximum time-window for nose-drooping the airfoil: is determined between 10^o up stroke and 10^o down stroke with the maximum deflection ($\Theta_{max} = 10^o$, Fig.1) at the maximum incidence of $\alpha=20^o$.
Numerical features of the Navier-Stokes code assumed for the calculation are:

Structured grid with 361x71 grid points
Spalart-Allmaras turbulence model
20 000 time-steps/period
calculation of two to three periods.

The calculations have been carried out fully turbulent. It is possible but not done in the present study to take into account transition in the unsteady calculation procedure as well, see [10],[11].

5. Transonic Airfoil Design

The numerical calculation utilizing the time-accurate Navier-Stokes code has been carried out in two steps:

1. In the perfect gas mode using the parameters of section 4.
2. In the fictitious gas mode using again the parameters of section 4.

Figs. 4 and 5 show some selected instantaneous Mach contours at the maximum Mach number M=0.73 and minimum incidence, $\alpha=0^o$, (Fig.4) and corresponding results at $\alpha=10^o$, M=0.5 during the up stroke motion. The white areas in Figs.4 and 5 correspond to supersonic flow in the

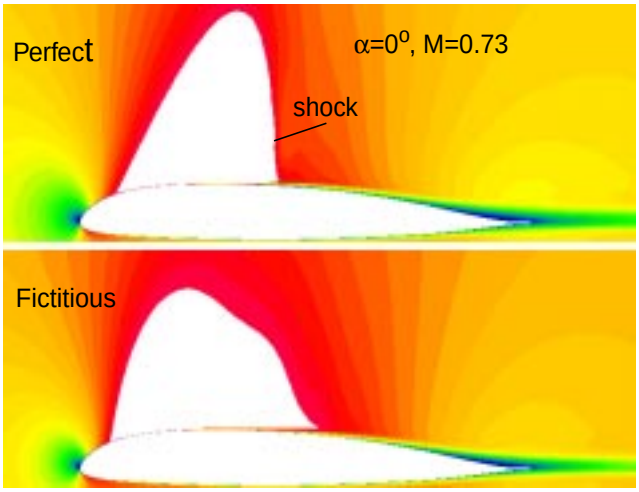

Fig.4 (upper) Basis Airfoil at Maximum Mach Number
Fig.4 (lower) Fictitious Gas Solution

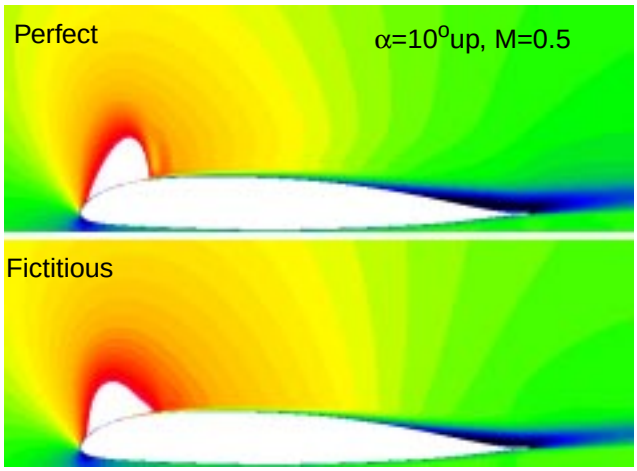

Fig.5 (upper) Basis Airfoil at Mean Incidence (up stroke) and Mean Mach Number
Fig.5 (lower) Fictitious Gas Solution

perfect gas mode and to the fictitious gas region in the FG-mode respectively. Figs. 4 and 5 both indicate that the downstream boundary of the FG-region does not show any sign of a shock wave.
To determine a modified airfoil shape utilizing the method of characteristics for each time step as has been outlined in section 3 would result in a time dependent shape variation. This will be very difficult to realize. Therefore only the time instant at the **maximum** Mach number (M=0.73, $\alpha=0^o$) as indicated in Fig.4 is used to modify the airfoil. In order to avoid a reduction of the airfoil thickness as it is shown in Fig.3 only a local modification at both upstream and downstream ends of the FG-area are modified by extended surface bumps. Fig.6 shows the shapes of the basis airfoil and the modified airfoil with the introduction of both ESB and RSB. The modified airfoil section has been

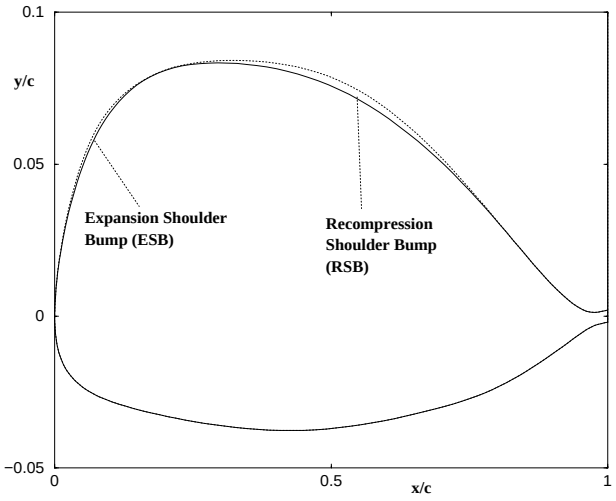

Fig.6: Shape Variation by ESB and RSB, modified Airfoil: A1581, y-Coordinate Enlarged

given the DLR internal nomenclature: **A1581**.
Fig.7 shows instantaneous pressure- and skin friction distribution for both basis airfoil and the modified airfoil including ESB- and RSB-bumps.
For the modified airfoil a slight reduction of the shock strength as well as a lift up of the skin friction in the shock region can be detected. These effects are also found within a time window adjacent to the maximum Mach number. It is expected that further improvements will be achieved by means of detailed variations of the bump shapes.

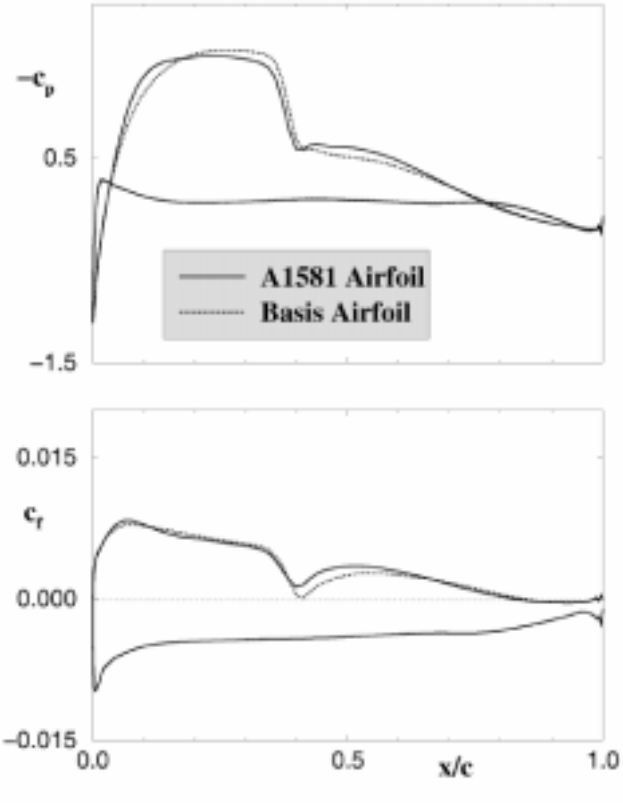

Fig.7: Instantaneous Pressure- and Skin Friction Distribution at M=0.73, α=0^o

6. Nose-Droop Design

The next step in the design loop of a new airfoil section is the introduction of a nose-drooping device following the design constraints of the wind tunnel model as given in Fig.1. The modified airfoil section A1581 which has been developed in section 5 will be used for this purpose.
The moving part of the airfoil as indicated in Fig.1 will be deflected by a maximum of Θ=10^o. For the numerical calculation the movement of the leading edge flap has to be discretized in such a way that a smooth time-dependent variation of the shape from the rigid airfoil A1581 to the maximum deflection angle is achieved. This variation is determined in a sinusoidal mode. Fig.8 shows the variation of shapes with 41 single steps which have been developed by means of the Geometry Generation Software, [12]. To implement the time dependent variation of the airfoil shape into the Navier-Stokes code it is necessary to use deforming grids [9], i.e. grids which are representing the instantaneous airfoil shape at each time instant. The grid is fixed to the outer rigid boundary which is 15 chord length away from the airfoil in all directions.
In the solution procedure the number of 41 single shapes is not sufficient. The necessary high resolution with respect to time makes an interpolation procedure necessary to determine the corresponding shapes for each time step. The intermediate shapes are determined by a linear interpolation procedure.

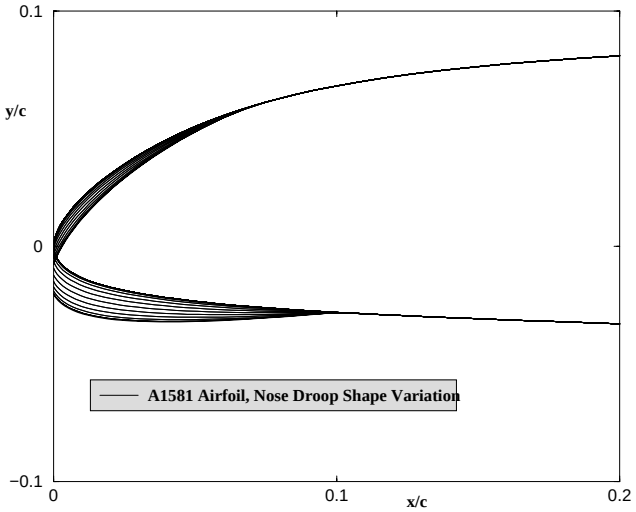

Fig.8: Airfoil Leading Edge Deformation: Nose-Drooping Device (41 Shapes)

Two additional parameters have to be specified to determine the time dependent variation of the leading edge droop in detail:

- Time-window where the deformation is taking place
- shape of time-dependent deformation

The time-window is placed between the mean incidence at 10^o up stroke (T=0, T corresponds to the normalized time) and the mean incidence at 10^o down stroke (T=0.5) with the maximum deformation at the maximum incidence, i.e. at 20^o (T=0.25) in the present case. It will be shown in the discussion of results that this time window extension and location inside the loop gives the optimum results compared to other arrangements.

The shape of time-dependent deformation is chosen to be sinusoidal: starting smoothly from the basis airfoil shape to the maximum deformation and taking the reversed way towards the basis airfoil, i.e. defining a sinus wave for the deformation inside the chosen time window.

7. Discussion of Results

7.1 Force- and Moment Loops

Fig.9 displays lift-,drag- and pitching moment loops versus incidence for the basis airfoil and the drooping airfoil respectively. In the drooping case two different extensions of the time window in which the drooping takes place is investigated. In one case (dotted curve) the time window is extended between 10^o up stroke and 10^o down stroke with the maximum deformation (maximum droop, see Fig.8) at the maximum incidence, $\alpha=20^o$.

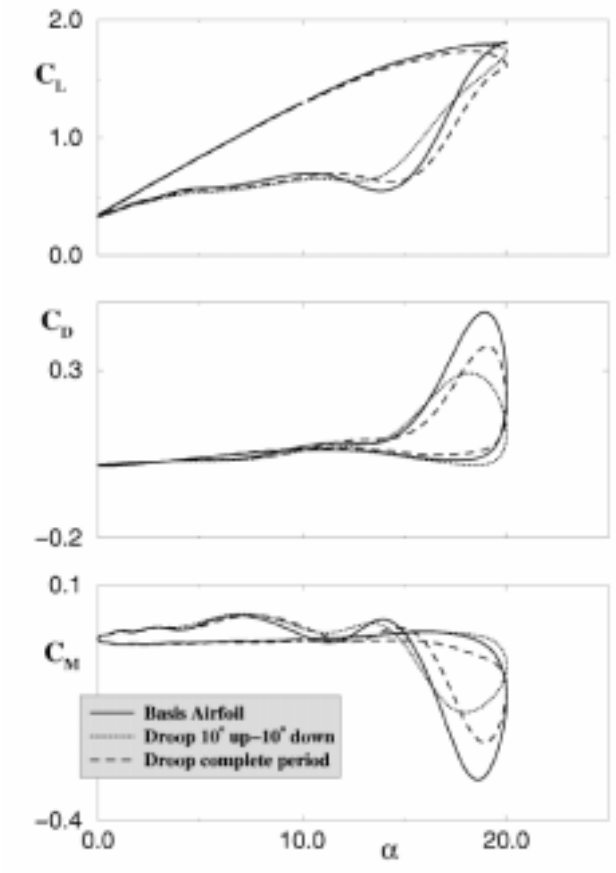

Fig.9: Lift-,Drag- and Pitching Moment Hysteresis Loops for Basis and Drooping Airfoils

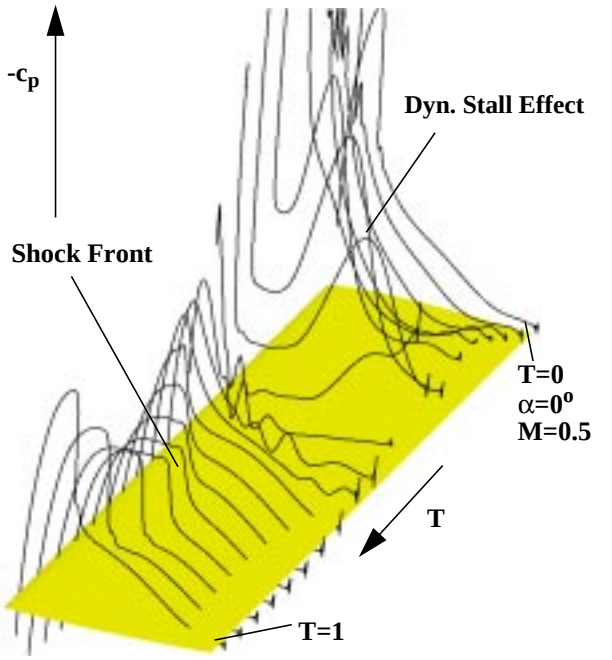

Fig.10: Time Dependent Development of Pressure Distributions Versus Time; Basis Airfoil

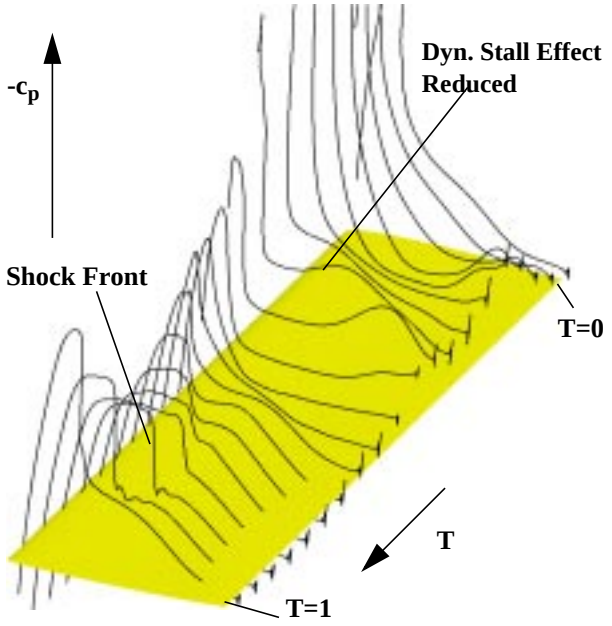

Fig.11: Time Dependent Development of Pressure Distributions Versus Time; A1581 Airfoil with Droop

In the second case (dashed curve) the time window with droop is extended over the whole period again with the maximum droop at $\alpha=20^o$.
It is obvious from Fig.9 that the extension of the time window between T=0 and 0.5 is an optimum: The maximum lift of the drooping airfoil is only slightly reduced compared to the rigid airfoil. On the other side the maximum drag of the drooping airfoil is reduced by about 40% and the minimum pitching moment shows a similar reduction of nearly 50%. Numerical experiments have shown that other arrangements of the drooping time window do not improve the results: A shift of the maximum droop either into the up stroke or into the down stroke does not show improvements.

7.2 Pressure Distributions

The development of the unsteady surface pressures over one period of airfoil oscillation are indicated in Figs. 10 and 11 for the rigid basis airfoil (Fig.10) and the modified and drooping airfoil A1581 (Fig.11). The rigid basis airfoil shows very strong extra pressure peaks developing over the upper surface towards the trailing edge. These pressure peaks are caused by the dynamic stall vortex travelling over the upper surface of the airfoil. Severe pressure fluctuations occur at about T=0.5 after the dynamic stall vortex has left the airfoil surface. During the second half of the period a shock front is developing. The shock starts close to the leading edge and travels downstream until it reaches its extreme position at M=0.73, $\alpha=0^o$.
In the drooping airfoil case, Fig.11, the same events as have been discussed for the rigid airfoil can still be detected. But now it is quite obvious that the extra peaks due to the effect of the dynamic stall vortex are considerably reduced (see Fig.11 for details). The transition from the high incidence region to the high Mach region, i.e. beyond T=0.5 shows a smooth variation of pressures.
The shock strength at about the maximum Mach number (M=0.73 at T=0.75) is only slightly reduced as has been outlined already in detail in Fig.7.
As has been mentioned before with some additional effort it will be possible to also improve the flow features in the transonic region and reduce the shock strength correspondingly.
Fig.12 (rigid basis airfoil) and Fig.13 (drooping airfoil) show some selected pressure- and skin friction distributions during the down stroke motion of the airfoil between T= 0.25 and T=0.5. The curves indicate the upper surface distributions only.
The effect of the dynamic stall vortex and its movement over the airofoil upper surface is clearly detectable for the basis airfoil in Fig.12. In the drooping airfoil case (Fig.13) the pressure distributions show only a moderate extra pressure peak starting more downstream beyond mid section of the airfoil. However it is clearly visible that a dynamic stall vortex still exists. The skin friction distributions show a similar behavior in both figures: In the down stroke region the flow is almost completely separated where the separation region starts further downstream in the drooping case.
With decreasing incidence the flow reattaches from the leading to the trailing edge continuously.
A special flow feature can further be seen during the second half of the oscillation period between T=0.75 and T=1 in Fig. 10 and 11. Within this time frame the shock is moving up stream due to the increase of incidence and continuous reduction of the Mach number. The shock wave is steepening during this phase and some pressure fluctuations occur. These fluctuations can also be detected up stream of the airfoil and may be the source of noise development during this part of the loop.

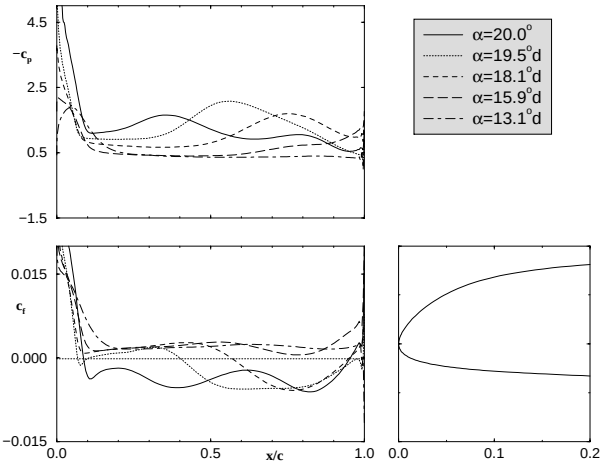

Fig.12: Selected Pressure- and Skin Friction Distributions during Down Stroke: Basis Airfoil

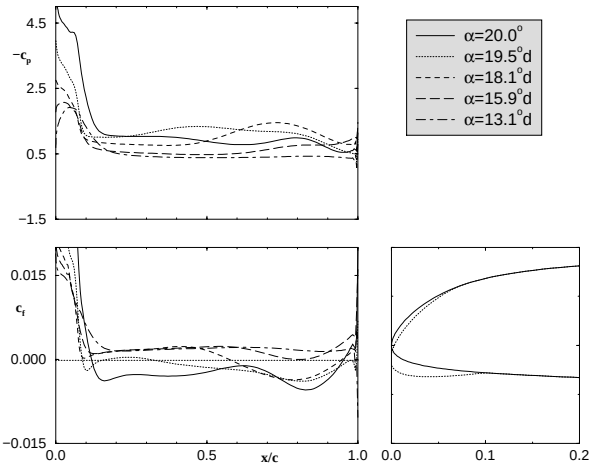

Fig.13: Selected Pressure- and Skin Friction Distributions during Down Stroke: Drooping Airfoil

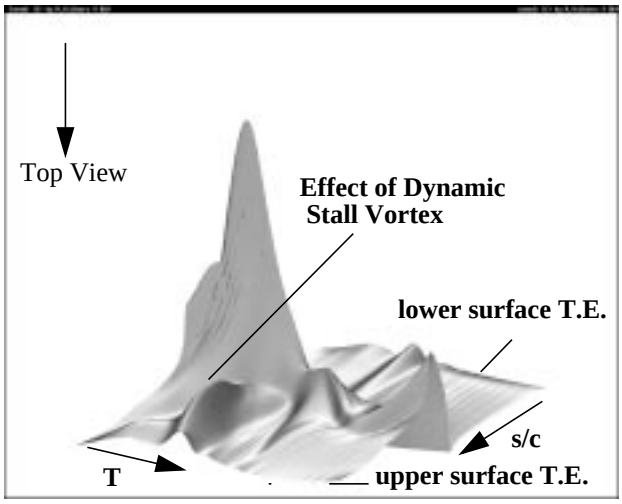

Fig.14: Pressure Mountain versus s/c and T; Rigid A1581 Airfoil

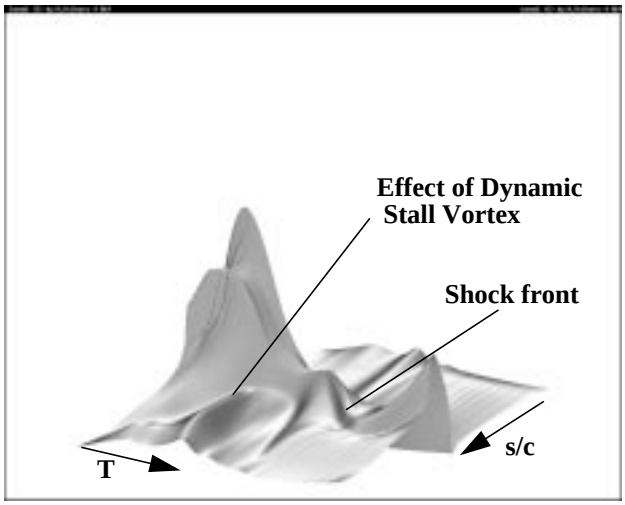

Fig.15: Pressure Mountain versus s/c and T; Drooping A1581 Airfoil

In addition to the pressure plots in line mode of Figs. 10 to 13, Figs.14-16 show pressure distributions as mountain plots over a plain determined by the surface coordinate s/c (from lower surface to upper surface trailing edge, see indications in Fig 14) as one coordinate and the normalized time T as the second coordinate.
Fig. 14 displays the result of the rigid A1581 airfoil, Fig.15 shows the corresponding result for the drooping airfoil. The most important differences of both pressure mountains are

- a large reduction of the leading edge pressure peak
- a reduction of the secondary pressure peak due to the dynamic stall vortex
- similar effects due to the moving shock front.

The latter event can be studied in more detail in Fig.16 indicating the top view of Fig.15 (drooping A1581 airfoil). The shock front is starting close to the airfoil leading edge and is moving downstream and again up stream similar to a sin wave.
The effect of the dynamic stall vortex is also clearly indicated. It is much smoother in the present drooping airfoil case compared to the rigid airfoil (see Fig.14).
The trace of the extra pressure peak caused by the dynamic stall vortex shows almost a straight line in the space-time domain. The inclination of this trace with respect to the s/c-coordinate is a measure of the travel speed of the dynamic stall vortex over the airfoil upper surface. In the present cases this speed is about 25% of the main flow velocity.

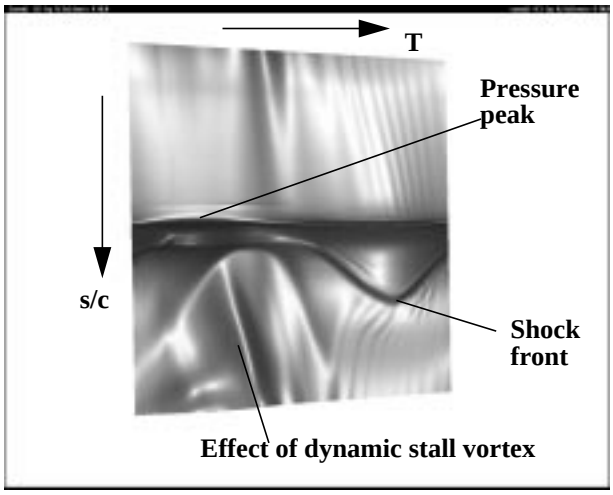

Fig. 16: Pressure Versus s/c and T, Drooping A1581 Airfoil; Top View of Fig.15

7.3 Flow Field Characteristics

The previous sections have shown the effects of the unsteady flow on the pressure- and skin friction development as well as on the overall forces and moment of the rigid and deforming airfoil respectively. To better understand these effects it is necessary

- to investigate the complete unsteady flow field
- to explore the effects of time-dependent pressure-, Mach number-, vorticity-distributions, etc. over the complete space and time domain
- to follow these developments by means of movie sequences

The latter aspect is of major concern to better understand the physical aspects involved in the present problem. Therefore a number of movie sequences have been developed showing pressure-, Mach- and vorticity-distributions either in the space fixed (inertial) or in a body fixed system respectively.
Only if the complex physics of the flow is completely understood it will be possible to find an optimum design methodology for dynamic stall and shock control.

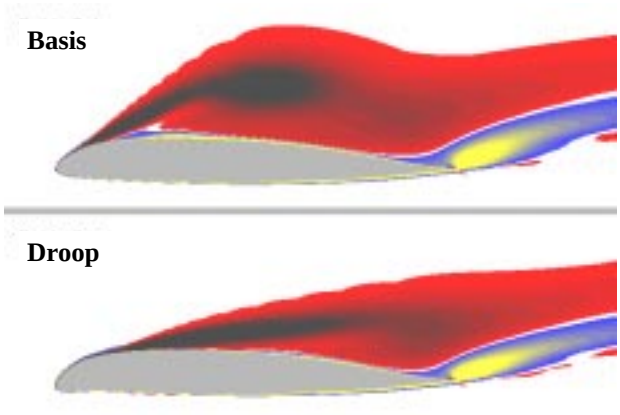

Fig.17: Instantaneous Vorticity Distribution at T=0.25 (α=20^o, M=0.27);
Upper Figure: Rigid Airfoil
Lower Figure: Drooping Airfoil, (Maximum Droop)

7.4 Vorticity Management

Fig. 17 shows the instantaneous vorticity distribution at the maximum incidence (α=20^o) and minimum Mach number (M=0.27) respectively. The formation of a dynamic stall vortex is visible in both figures. However the vortex strength and its extension into the flow field is considerably reduced in the drooping case. In the rigid airfoil case the dynamic stall vortex is lifted away from the surface after a reversed flow area has been developed along the upper surface and a counter rotating vortex (counter clockwise) is formed at the trailing edge. In the drooping airfoil case these effects are not completely avoided but have been smoothed. The effects can be studied on forces and moment loops (Fig.10) as well as on the different displays of pressure distributions (Figs.11-16).

It can further be seen in Fig.17 that the start of the vortex i.e. the separation of vorticity from the airfoil surface into the flow starts at the very leading edge of the rigid airfoil whereas the point of vorticity separation is shifted in the drooping case to the end of the droop device (about 10% chord).

In [13] it has been outlined in detail that a proportionality exists between the adverse pressure gradient on the airfoil upper surface and the vorticity flux normal to the surface expressed by

$$\frac{\partial p}{\partial s} \sim \frac{\partial \Omega}{\partial n} \qquad \text{Eq.1}$$

with s as the airfoil surface coordinate, n as the surface normal and Ω as the vorticity strength. Eq.1 does also apply for moving bodies.

Eq.1 indicates that the production of vorticity is high where the adverse pressure gradient is high, i.e. close to the airfoil leading edge. A similar relationship exists between the adverse pressure gradient and the curvature of the airfoil. The airfoil leading edge is the part of the airfoil with the highest curvature. It follows that the three quantities:

- curvature
- adverse pressure gradient
- vorticity flux

are in direct relationship to each other. If this fact is understood well then definite design rules for the airfoil leading edge deformation can be specified to control the production and convection of vorticity during the time-dependent motion of the airfoil.

Fig.18 shows again the A1581 airfoil with the 41 steps of nose-droop deformation where the y-coordinate is highly enlarged. The figure shows very clearly that the curvature along the airfoil leading edge is redistributed and shifted towards the lower surface of the airfoil. Due to the local reduction of the curvature on the upper surface leading edge the corresponding adverse pressure gradient over large portions of the time period is reduced specifically during the high incidence part of the loop. The vorticity flux, i.e. the production of vorticity along the upper surface leading edge, is reduced subsequently. As long as the vorticity production is low it can be convected through the boundary layer towards the trailing edge and the flow keeps attached. If the vorticity production is too high it will be accumulated at the leading edge to form a large concentrated vortex which as a consequence will then start to travel along the surface and finally lift off the surface to start the breakdown of the airfoil lift and increase drag and pitching moment correspondingly.

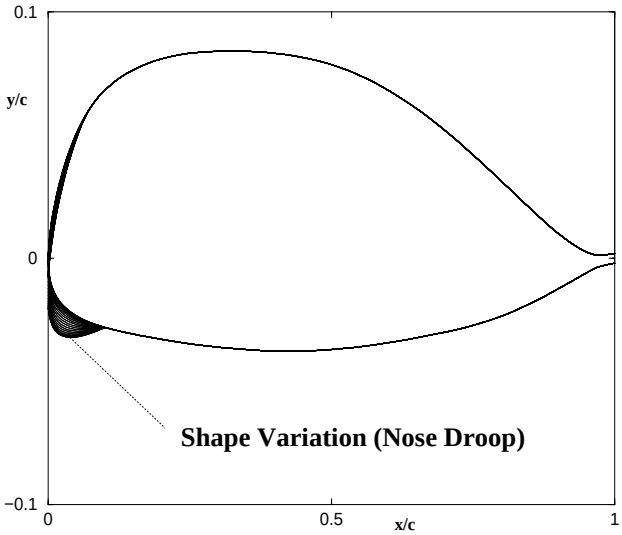

Fig.18: Leading Edge Modification (Nose-Droop) on the A1581 Airfoil, Details see Fig.8

Fig.17 shows that a concentrated vortex could not completely be avoided but the vortex strength could at least be reduced considerably. Without the constraints given by the blade manufacturers (10% deflection area, 10^o deflection angle, Fig.1) further improvements can be achieved by means of the rules given before.

8. Conclusions, Future Activities

The wind tunnel blade model which will be developed within the scope of the german project AROSYS (Adaptive Rotor Systems) will have a dynamic leading edge flap of 10% chord with $\Theta=10^o$ maximum deflection angle. In the present paper numerical calculations have been carried out to simulate the oscillating and deforming blade by means of a time accurate Navier-Stokes code. It is shown that the present amount of deformation is already suitable to reduce the effects of dynamic stall considerably. Keeping the maximum lift at the same level as in the rigid airfoil case drag and pitching moment extreme values are reduced by nearly 50%.

It has further been demonstrated that a redesign of the basis airfoil incorporating transonic design methodology further improves the airfoil characteristics on the advancing side of the loop.

Upcoming new structural devices based on active fiber or active patches directly integrated into the blade surface may either twist the rotor blade or may alternatively deform the airfoil camber (active camber) as indicated in Fig.19. The already existing numerical software used in the present study can also be applied for this type of sophisticated devices.

The calculations outlined in the present paper are based on fully turbulent flow assumptions. It has been discussed in [10] that the introduction of a transition model even in the time dependent code is straightforward and gives improvements compared to experimental data.

In future efforts the aspect of transition which is of major concern for the dynamic stall and stall control problems will be investigated in more detail.

It is of further interest to extend the codes towards investigation of 3D-flows. First steps into this direction have also already been taken.

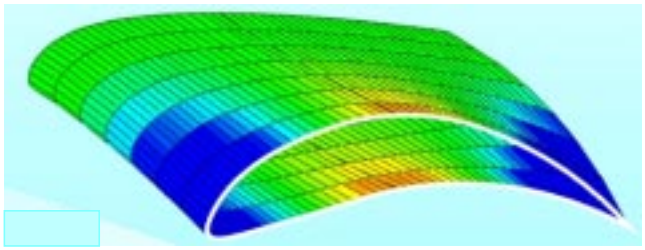

Fig.19: Flexible Camber Airfoil Section without Kinks and Gaps

9. References

[1]Schimke,D.,Jänker,P.,Wendt,V.,Junker,B.,"Wind Tunnel Evaluation of a Full Scale Pieco-Electric Flap Control Unit", 24th European Rotorcraft Forum,15-17 Sept.,1998,Marseilles,France.

[2] Lorkowski,T.,Jänker,P.,Hermle,F.,Storm,M.,Christmann,M.,Wettemann,M.,"Development of a Piezoelectrically Actuated Leading-Edge Flap for Dynamic Stall Delay", Twentyfifth European Rotorcraft Forum, Sept. 14-16,1999, Rome,Italy

[3]Geissler,W.Sobieczky,H.Vollmers,H.,"Numerical Study of the Unsteady Flow on a Pitching Airfoil with Oscillating Flap" 24th European Rotorcraft Forum, 15-17th September,1998, Marseilles, France, Paper AE09

[4] Sobieczky,H., Seebass,A.R., "Supercritical Airfoil and Wing Design", Ann.Rev.Fluid Mech.16,pp.337-363 (1984).

[5] Chandrasekhara,M.S., Wilder,M.C., Carr,L.W., "Unsteady Stall Control Using Dynamically Deforming Airfoils", AIAA-Paper 97-2236, June 23-25, 1997, Atlanta,GA.

[6] Chandrasekhara,M.S., Wilder,M.C., Carr,L.W., "Unsteady Stall Control Using Dynamically Deforming Airfoils", AIAA Journal,Vol.36,No.10,October 1998.

[7] Trenker,M.,Geissler,W.,Sobieczky,H.,"Airfoils with Dynamic Transonic Flow Control",18th AIAA Applied Aerodynamics Conference,Aug. 14-17,2000, Denver,CO.

[8] Li,P.,Sobieczky,H.,"Computation of Fictitious Gas Flow with Euler Equations",Acta Mechanica (1994) [Suppl] 4:251-257,Spriger-Verlag 1994.

[9] Geissler,W.,"Instationäres Navier-Stokes Verfahren für beschleunigt bewegte Profile mit Ablösung (Unsteady Navier-Stokes Code for Accelerated Moving Airfoils Including Separation)" in german, DLR-FB 92-03 (1992).

[10] Geissler,W., Chandrasekhara,M.S., Platzer,M., Carr,L.W.,"The Effect Of Transition Modeling On The Prediction Of Compressible Deep Dynamic Stall", 7th Asian Congress of Fluid Mechanics, Dec. 8-12, 1997, Chennai (Madras), India.

[11] Geissler,W., Carr,L.W., Chandrasekhara,M.S., Wilder,M.C., Sobieczky,H.,"Compressible Dynamic Stall Calculations Incorporating Transition Modeling For Variable Geometry Airfoils", 36th AIAA Aerospace Meeting and Exhibit, January, 12-15, 1998, Reno Hilton, Reno, NV.

[12] Sobieczky,H.,"Geometry Generator for Aerodynamic Design", CISM Course and Lectures No. 366, 'New Design Concepts for High Speed Air Transport', Springer, Wien,New York (1997), pp. 137-158.

[13] Reynolds,W.C.,Carr,L.W.,"Review of Unsteady Driven, Separated Flows",Paper AIAA Paper 85-0527, March 1985.